

Parison Formation and Inflation Behavior of Polyamide-6 During Extrusion Blow Molding

ALAN H. WAGNER* and DILHAN M. KALYON

*Highly Filled Materials Institute
Chemical Sciences & Engineering
Stevens Institute of Technology
Hoboken, New Jersey 07030*

Parison formation and inflation behavior of three polyamide 6 resins during extrusion blow molding were investigated using cinematography, a transparent mold, a pinch-off mold and a modified blow pin, which allowed the pressure inside the parison to be determined during inflation. The glass fiber filled polyamide exhibited negligible extrudate swell and significant drawdown, whereas polyolefin modified polyamide exhibited appreciable extrudate swell and relatively small drawdown effects. The inflation behavior of the polyolefin modified polyamide was similar to the behavior of conventional blow molding grade polyolefins, whereas the unmodified and glass filled polyamides exhibited different inflation characteristics. Their inflation behavior at different internal pressures was characterized by decreasing and increasing Hencky strain rates with inflation time at high and low internal blow pressures, respectively. The characterized parison formation and inflation behavior of the polyamides emphasize the importance of rigorous blow moldability experiments and the difficulties associated with linking various rheological material functions to the blow moldability of modified polyamides.

INTRODUCTION

Extrusion blow molded articles made of engineering resins are replacing traditional materials in more demanding applications. For example, automotive applications, including heating, ventilation, and air conditioning (HVAC) ducts and tanks, require exact tolerances to be met for satisfactory performance. In blow molding, it is important to control the final dimensions, including wall thickness, of the blow molded part. The dimensions are affected by the dynamics occurring during the three stages of the blow molding process: formation of the parison; inflation of the parison; and cooling of the shaped article. The dimensions of the shaped article are determined by the dimensions of the parison just prior to inflation, the geometry of the mold, and the deformation occurring during the inflation stage.

The extrusion of the parison out of an annular die (*Fig. 1*) and the changes in the dimensions of the free standing parison under the combined effects of swell and sag are complicated (1-7). Both sag and swell effects are time and temperature dependent. Various studies of mathematical modeling of extrudate swell of Newtonian, Generalized Newtonian and nonlinear vis-

coelastic fluids have been published (8-22). However, numerical modeling efforts have generally only attempted to predict the equilibrium extrudate swell values, whereas the development of the parison dimensions is sensitive to the time elapsed outside the die (1, 4).

Experimental techniques are still used to determine the transient swell behavior of the extrudate and a number of techniques are available. One of the earliest experimental methods for determining parison behavior during blow molding was developed by Sheptak and Beyer (23). They designed a special mold (*Fig. 2*) that divided the parison into twelve equal (25 mm) sections or pillows. From the pinched-off parison one could measure the width of the parison at 25 mm intervals as well as the weight of each pillow.

Parison swell behavior can be characterized in terms of the weight swell, S_w , diameter swell, S_D , and thickness swell, S_T :

$$S_w = \frac{4W_i}{\pi(D_o^2 - D_i^2)\Delta L\rho} \quad (1)$$

where ρ is the density of the melt, W_i is the weight of the i th parison pillow with length ΔL , and D_o and D_i are the outside and inside diameters of the die. The conventional procedure for determining the diameter swell, S_D , from the pinch-off mold data is to assume

* Currently with Allied Signal Inc., Morristown, N.J.

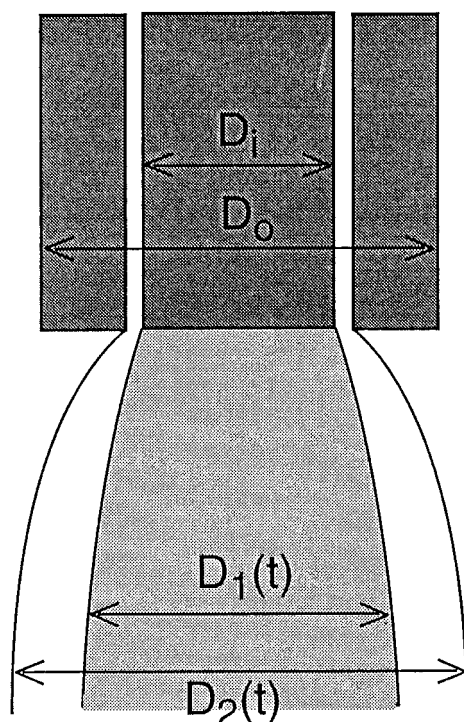


Fig. 1. Schematic representation of extrudate swell from annular die.

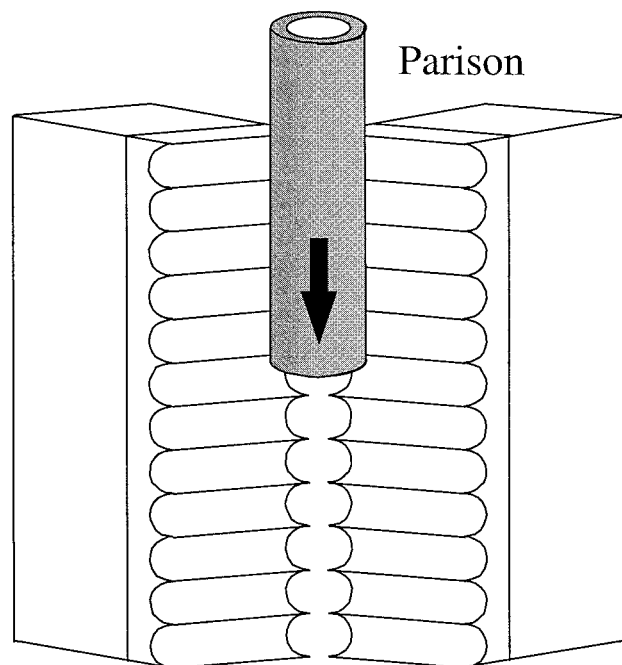


Fig. 2. Parison pinch-off mold.

that the width of the pinched-off parison represents one half the circumference of the parison prior to pinch-off (23):

$$S_D = \frac{2W_{LF}}{(\pi D_o)} \approx \frac{D_2}{D_o} \quad (2)$$

where W_{LF} is the lay-flat width of the pinched-off segment, D_o is the outer diameter of the die, and D_2 is the outer diameter of the parison before pinch-off. However, the assumption of a constant relationship between the lay-flat width and parison diameter is not valid: the relationship changes with parison thickness. As shown by Kalyon *et al.* (1) a photographic calibration is needed to determine accurately the parison diameter swell from pinch-off data. Kalyon *et al.* have characterized both the weight swell and diameter swell independently, and have obtained the third swell parameter, thickness swell (S_T), from the following:

$$S_W = S_D S_T \quad (3)$$

In Eq 3 it is assumed that the thickness of the parison and the die gap are small compared with the outside diameter of the parison and the die diameter. The parison pinch-off mold and video analysis were utilized extensively by Kalyon *et al.* (1, 4) to characterize the distributions of the diameter, thickness, and weight swell values in the extrusion blow molding process. The relationships between diameter and thickness swell upon capillary flow were investigated by Garcia-Rejon and Dealy (2) using optical techniques and in the absence of gravitational effects for high-density polyethylene and polypropylene. Other measurement techniques include movable photocell arrangements for measuring total parison length (24), video measurements (25), and recently, noncontact optical methods (26–29).

Parison inflation is the planar extension of a non-uniform viscoelastic polymer tube. End effects are significant, and strain rates vary throughout the inflation (30). Kamal *et al.* (30) utilized a transparent mold and cinematography to characterize for the first time the inflation dynamics where the dimensions of the inflating parison were determined as a function of time and the prevailing Hencky strain rates were obtained. The dimensions of the inflating parison were also obtained by Ryan and Dutta (31) under conditions in which the mold was not present. The dynamics of the inflation of elastic and viscoelastic cylindrical tubes have been analyzed (32–38). Recently, DiRaddo *et al.* (39) have studied the inflation of non-axisymmetric parisons, while Garcia-Rejon and DiRaddo (40) reported on the inflation of axisymmetric parisons into non-axisymmetric molds.

The objective of this work was to study the parison formation and inflation dynamics of the continuous blow molding process using unmodified and modified polyamide 6 resins. The rheological functions and the extrudate swelling (in the absence of gravitational effects) of the three resins were characterized in detail. The parison formation during blow molding was studied using parison pinch-off together with cinematography following Kalyon *et al.* (1). The inflation dynamics were characterized by employing a detailed motion analysis of the inflating parison using a transparent mold and cinematography to measure the inflation velocity and Hencky strain rates on the one hand, and

the internal inflation pressure of the parison on the other hand. Although several earlier studies (25, 30) have reported the line pressure near the blow pin during inflation, to our knowledge the pressure change inside the parison during inflation was not previously reported. A pressure transducer was also installed flush with the mold cavity. Thus, the true pressure difference between the inside and outside during the inflation stage of the blow molding process could be determined. Further, to our knowledge, there are no extensive data in the literature on the blow moldability of unmodified and modified polyamides. This study should help fill that gap.

EXPERIMENTAL EQUIPMENT AND PROCEDURES

A Krupp-Kautex model KEB2-14 continuous extrusion blow molding machine was employed in this study. As shown in Fig. 3, a convergent/divergent bushing and pin system was used to form the parison. The pin position could be controlled via a Hunkar parison programmer (model LAB# 311-1A) to yield a custom parison profile. The Hunkar parison programmer was set to produce a flat or uniform profile. An electrically heated, tungsten blade hot knife was used to properly cut the parison from the die.

Three molds and a custom designed blow pin were utilized in this study. A parison pinch-off mold based on the design of Sheptak and Beyer (23), was constructed to study the parison formation and swell/sag behavior of the resins. The mold consisted of two stainless steel plates $330.2 \times 152.4 \times 25.4$ mm, which had twelve 25-mm semicircular grooves machined across each face such that when the two plates were brought into contact, twelve circular cavities were formed. The temperature of this mold could be regulated via the circulation of temperature-controlled water.

To study the clamping and inflation stages in the blow molding process, a transparent mold was built according to the design used by Kamal *et al.* (30). The

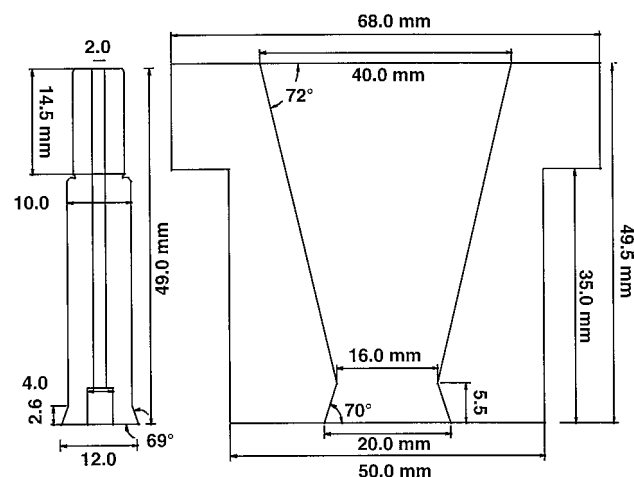


Fig. 3. Mandrel and die bushings used in continuous blow molding.

two mold halves were machined out of aluminum such that each would accommodate a half cylinder of Corning Pyrex brand glass tubing with an outside diameter of 88.9 mm and a wall thickness of 4.7 mm with an overall length of 220 mm. Silicone sealant was used to both hold the glass inserts in place and to compensate for the differences in thermal expansion between the glass and aluminum. The mating surface of one mold half was machined to allow for venting of the trapped air during inflation of the parison and prevent the shattering of the glass inserts resulting from excessive pressure buildup of the trapped air. The top of each aluminum mold half was machined to accept the standard neck tooling, which was removed from the commercial mold. The bottom of each aluminum mold half was machined to receive two semicircular pieces of flat Pyrex glass. Two aluminum bottom bars were prepared to pinch-off and seal the bottom of the parison as well as hold the bottom glass in place. To prevent excessive glare while filming, the mold surfaces were painted with a heat-resistant matte black coating.

The third mold used in this study was a standard cylindrical mold that produced cylindrical samples with diameters of 65 mm and lengths of 175 mm. This mold was modified to contain an Omega Engineering Inc. flush diaphragm pressure transducer model PX102 (0 to 100 psig range) in one mold half and a RdF Corp. Micro-Foil heat flow sensor/thermocouple (RdF #20457-1) in the other half.

A custom blow pin was designed and built that permitted the measurement of the pressure in the parison while the parison was inflating. An aluminum blow pin was machined to house a Lucas NovaSensor solid state pressure transducer model NPH-8-700AH. As illustrated in Fig. 4, the tip of the blow pin was designed to allow the blow air to pass through the transducer without giving a false reading while still inflating the parison.

Parison growth, swell, and sag were documented utilizing the parison pinch-off mold in conjunction with motion analyses. The parison dimensions were recorded with our CCD cameras, principally a Cannon L1, Hi8 mm video camera/recorder with a zoom lens. The camera was calibrated by suspending a series of cylinders with known diameters.

During extrusion, a tube of resin was continuously extruded through the die gap under steady melt temperature and head pressure conditions. When the parison reached the bottom of the pinch-off mold, the mold was closed and the parison was pinched into twelve 25-mm sections or pillows. Each chain of pillows was removed, numbered, separated, weighed, and measured. The video image of the parison was subsequently analyzed for the outside diameter versus axial location profile of the parison just prior to mold closing.

The clamping and inflation stages of the continuous extrusion blow molding process were studied by employing the transparent mold in conjunction with video analyses and pressure recording blow pin. In

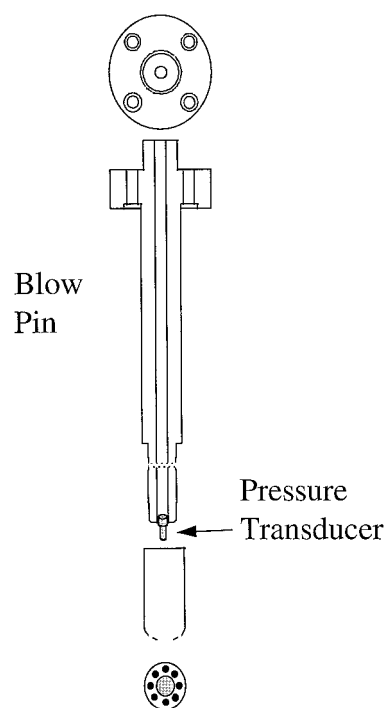


Fig. 4. Modified blow pin with pressure transducer.

this second set of experiments, the transparent mold and the blow pin containing the pressure transducer were mounted on the blow molding machine. Two video cameras (Cannon L1, 8 mm video camera/recorder and Chinon model C8-C60, CCD equipped with a 6:1 zoom lens and auto-aperture control) were situated to record the clamping and inflation of the parison from the front and from below. A mirror positioned 45° from vertical was used to view the bottom of the mold during inflation.

A continuous tube of resin was extruded until melt temperature and head pressure had stabilized. Upon reaching equilibrium, the tube was cut, allowing a new parison to form. When the parison was of sufficient length, the mold closed around the parison and the parison was severed from the die. The blow pin was inserted into the parison and the parison inflated. Upon cooling, the mold was opened and the bottle was removed and saved. The entire process was recorded on video tape for subsequent image analysis. Additional information on the inflation dynamics of the parison was obtained from the cooling dynamics experiments by studying the pressure traces from the transducer pairs located in the blow pin and the instrumented mold wall.

MATERIALS

The blow moldability of three polyamide resins was studied. The first polyamide is a chain extended, multi-branched, natural colored polyamide 6. This resin will be referred to as the "neat" resin. The second polyamide resin is a chain extended, multi-branched polyamide 6 containing 12 wt% chopped glass fibers and carbon black. The glass fibers had a diameter of

10 μm and length over diameter ratio of 60. This resin will be referred to as "fiber-incorporated." The last polyamide is a polyolefin modified polyamide 6 also containing carbon black and will be referred to as "polyolefin modified." Various properties of the resins are listed in Table 1.

Polyamide is a relative newcomer to the blow molding industry because of its generally low viscosity and elasticity at typical processing temperatures. Recent developments in the manufacturing of polyamide have allowed the resin to possess greater melt strength, i.e., higher elasticity via the use of chain extenders, branching, blending, and filling. These three resins were chosen to assess the effects of processability modifiers on extrudate swell, parison development, parison inflation, and the general blow moldability of the resin.

RESULTS AND DISCUSSION

The variations of the swell parameters with distance from the die for the neat and fiber-filled polyamide resins are shown in Figs. 5 and 6. The data are reported in conjunction with 90% confidence intervals determined according to Student's *t*-distribution. The unmodified polyamide 6 exhibited a greater degree of nonuniformity along the axial direction (Fig. 5). The parison section adjacent to the die is affected by the physical presence of the die, which restricts swell, and there the parison has the shortest amount of time for swelling to occur before pinch-off. The diameter swell increased from 1.1 near the die to 1.3 at the bottom of the parison. Some necking of the parison due to draw-down is evident from the locations of the observed minima in thickness and weight swell.

The incorporation of 12 wt% glass fibers into a polyamide matrix resulted in the reduction of all swell parameters, as shown in Fig. 6. The values of the weight swell ratio are less than one, and thus indicate that the drawdown of the parison was significant during the parison formation process. The diameter swell of the fiber incorporated resin is only slightly greater than one, and the diameter swell is essentially constant along the axial direction of the parison. The thickness swell of the fiber incorporated resin is actually less than one, indicating a parison wall thickness

Table 1. Properties of the Polyamides Used in This Study.

Property	Fiber Polyolefin		
	Neat	Incorporated	Modified
Specific gravity	1.13	1.22	1.09
Tensile strength at yield (MPa)	85	117	59
Ultimate elongation (%)	180	—	175
Flexural strength (MPa)	110	166	72
Flexural modulus (MPa)	2895	4658	1915
Notched Izod impact (J/m)	55	42	267
Heat deflection temperature @ 246 psi (°C)	66	195	58
Melting temperature (°C)	215	—	215
Melt index	0.5–0.7*	3.5**	1.8*

* At 235°C, dead weight used is 1 kg.

** At 235°C, dead weight used is 10 kg.

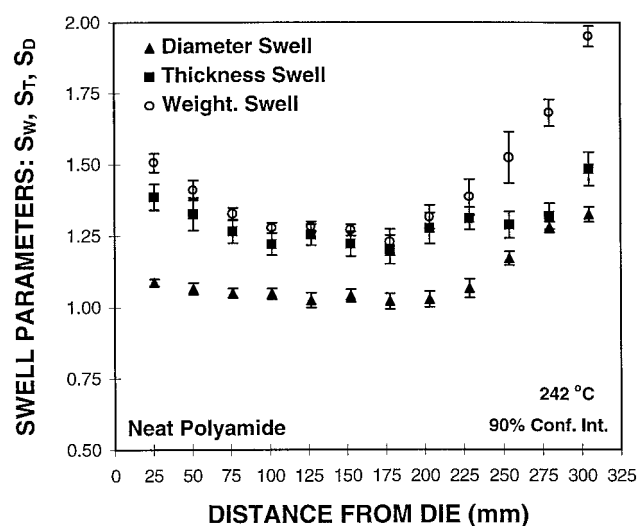


Fig. 5. Swell parameters for neat polyamide.

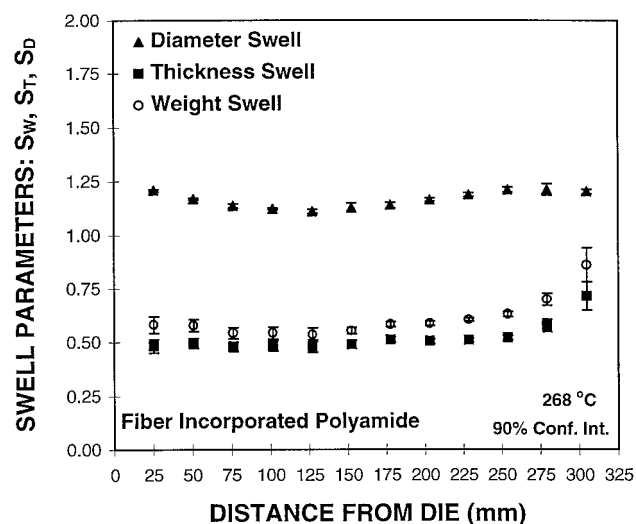


Fig. 6. Swell parameters for glass filled polyamide.

of less than the die gap. As indicated by Krolick (41), tooling with a wide gap is needed to process fiber filled resins.

The first normal stress difference, N_1 , versus the deformation rate behaviors of the neat resin and the glass filled resin are compared in Fig. 7, which indicates that the first normal stress difference behaviors of the two resins are similar. The storage modulus values of the two resins, shown in Fig. 8, are also close to each other. It is generally recognized that the first normal stress difference and storage modulus material functions represent the "elasticity" or the elastic energy storage capability of a polymer under sufficiently low strain rate and strain conditions. In the absence of solid particles, greater elasticity (as suggested by greater first normal stress difference or storage modulus) generally indicates a greater ability to hold shape and greater swell. However, here we have shown that the role played by the incorporation of the fibers is to reduce the swelling and increase the draw-

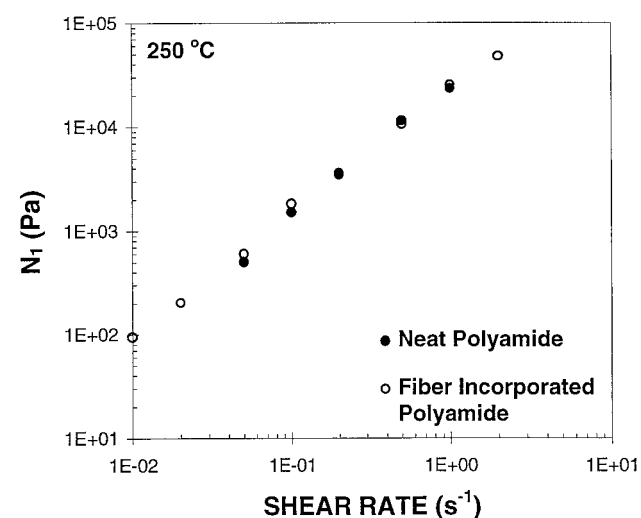


Fig. 7. First normal stress difference vs. shear rate for neat and glass fiber filled polyamides.

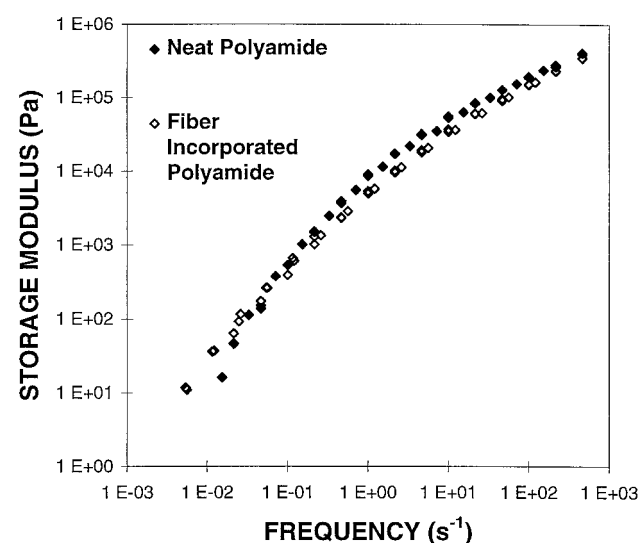


Fig. 8. Storage modulus vs. frequency for neat and glass fiber filled polyamides.

down or sag (because of the relative lack of ability for the parison to hold its shape) in spite of the observed similar behavior in the storage modulus and first normal stress difference values. Thus, tailoring of a blow molding grade resin to generate the desired swell behavior through the use of conventional rheological characterization techniques, i.e., storage modulus and first normal stress difference material functions, would lead to erroneous results when fibers are incorporated into the matrix.

The polyolefin modified polyamide 6 demonstrated the greatest amount of swell of all three resins, as shown in Fig. 9. Although the weight and thickness swell increase significantly with distance from the die, the resin has high enough "melt strength," i.e., elasticity, to resist necking and drawdown. Because of the greater swell behavior of the neat and polyolefin modified resins, it is possible to process them through

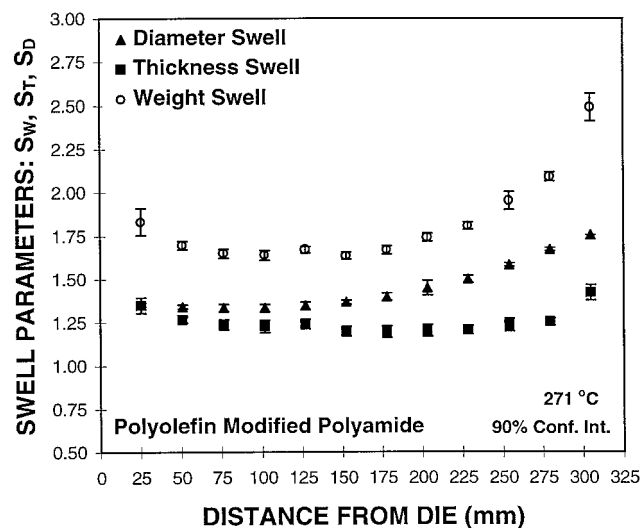


Fig. 9. Swell parameters for polyolefin modified polyamide.

tooling with a smaller die gap than needed for the fiber filled resin. Since the polyolefin modified resin is resistant to necking, much larger parisons, and hence parts, can be molded from this resin.

Capillary extrudate swell experiments carried out on the same three resins but under conditions that avoid sagging or drawdown effects (42) revealed the same relative swell behavior under similar temperature and wall shear rate conditions. The fiber incorporated resin had the smallest equilibrium capillary swell, $B(\infty) = 1.25$, the polyolefin resin exhibited the greatest degree of equilibrium swell, $B(\infty) = 1.75$, and the neat resin had intermediate equilibrium swell values, $B(\infty) = 1.65$. These results again indicate that the swelling of the polyamide is suppressed significantly because of the presence of the solid phase.

A power law relationship has been used to describe the dependence of weight swell values on the diameter swell values (43):

$$S_D = S_W^a \quad (4)$$

An exponent, a , value of 0.5 indicates isotropic expansion (i.e., the diameter swell increases at the same rate as the thickness swell) of the parison during parison formation prior to inflation. As shown in Fig. 10, for low weight swell values, the diameter swell of the neat polyamide resin is lower than expected based on isotropic expansion. The agreement is better at higher weight swell values. The relationship is independent of the temperature of the resin. On the other hand, the exponent a of the glass filled polyamide resin (Fig. 11) is a function of temperature. At both temperatures the diameter swell is much greater (or conversely, the thickness swell is much smaller) than what is predicted from the isotropic expansion of the parison.

However, in the range of temperatures and shear rates employed, the polyolefin modified polyamide exhibited essentially isotropic swell, as illustrated in Fig. 12. Kalyon and Kamal (4) determined that the exponent a for high-density polyethylene resins falls within

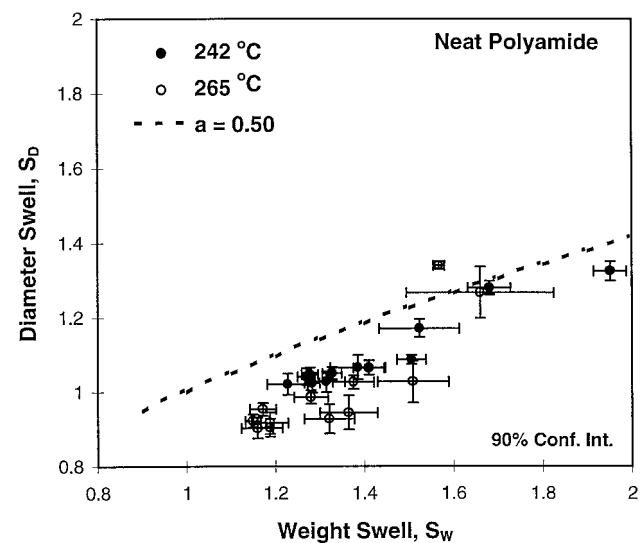


Fig. 10. Relationship between diameter and weight swell parameters for neat polyamide.

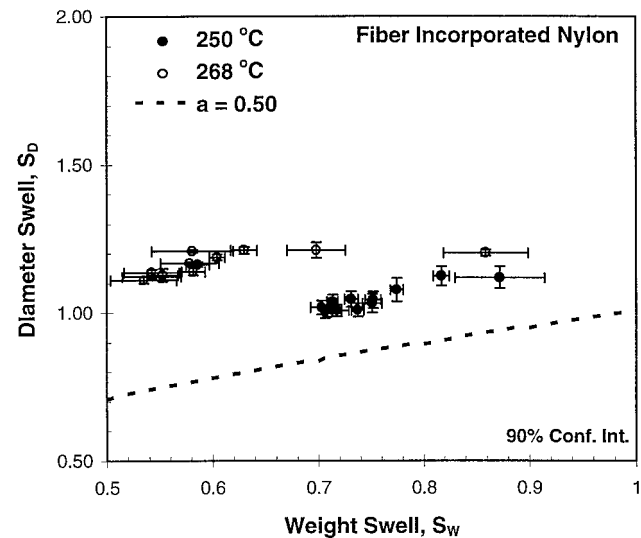


Fig. 11. Relationship between diameter and weight swell parameters for glass filled polyamide.

a small range between 0.55 and 0.61, suggesting that the diameter swell increases at a slightly greater rate than thickness swell for blow molding grade polyethylene resins. Similar values were determined by Garcia-Rejon and Dealy (2) and Orbey and Dealy (3) upon extrusion of polyethylene resins from straight annular and converging dies (10° taper angle) in the absence of gravitational sag effects.

The results reported Figs. 10 through 12 suggest that the fiber incorporated polyamide behaves very differently than the unmodified and polyolefin modified polyamides. Some of the differences are attributed to the orientation and the restraining effects of the glass fibers, which were reported earlier (42). Further, the presence of significant sag effects especially associated with this fiber incorporated resin resulted in values of exponent a that are close to zero.

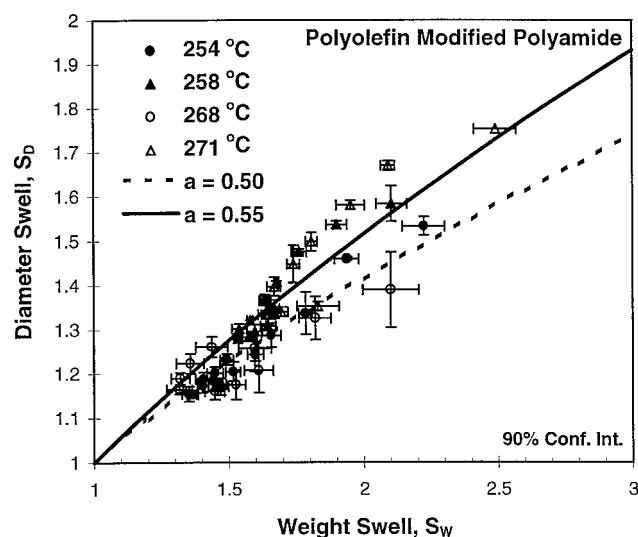


Fig. 12. Relationship between diameter and weight swell parameters for polyolefin modified polyamide.

The neat and fiber incorporated resins, at all inflation pressures, and the polyolefin modified resin, at high inflation pressures, had parisons that generally inflated by first expanding in the center or at locations close to the top until the parison was constrained by the mold wall. Once in contact with the mold wall, the parison inflated biaxially until the cavity of the mold was completely filled. The inflation behavior of the glass-filled polyamide 6 is shown in Fig. 13. A bulge in the profile of the inflating parison is observed (4–6 cm from the top) and the top portion of the cavity is cov-

ered by the melt sooner than the bottom. Parisons of the polyolefin modified resin did not expand in the middle first but rather expanded uniformly, as shown in Fig. 14, at the low inflation pressure. This inflation behavior is similar to the inflation behavior of high density polyethylene resins studied by Kamal *et al.* (30). The durations required for the center of the parison to reach the mold wall are given in Table 2. For both nominal inflation pressures, parisons of glass-filled polyamide reach the wall faster than the neat and polyolefin modified polyamides.

The progression of the outside diameter of the parison, $D_2(t)$, for all three resins at the center of the mold is shown in Fig. 15. For the neat and fiber incorporated resins at high inflation pressures and the polyolefin modified resin at high and low inflation pressures, the inflation proceeds with an approximately constant rate ($dD_2(t)/dt$). This is similar to the behavior observed by Kamal *et al.* (30) for high-density polyethylene resins. However, at lower pressures, the neat and fiber incorporated resins exhibit a delay or lag in inflation while the internal pressure increases.

The corresponding effective Hencky strain rates:

$$\dot{\epsilon}(t) = \frac{1}{D_2} \frac{dD_2(t)}{dt} \quad (5)$$

are plotted in Fig. 16. For the parisons exhibiting an approximately linear increase in diameter with time, the corresponding strain rates start out high and decrease monotonically throughout the inflation stage. The parisons that inflate at a slower rate initially have a much lower strain rate at the onset, followed by a

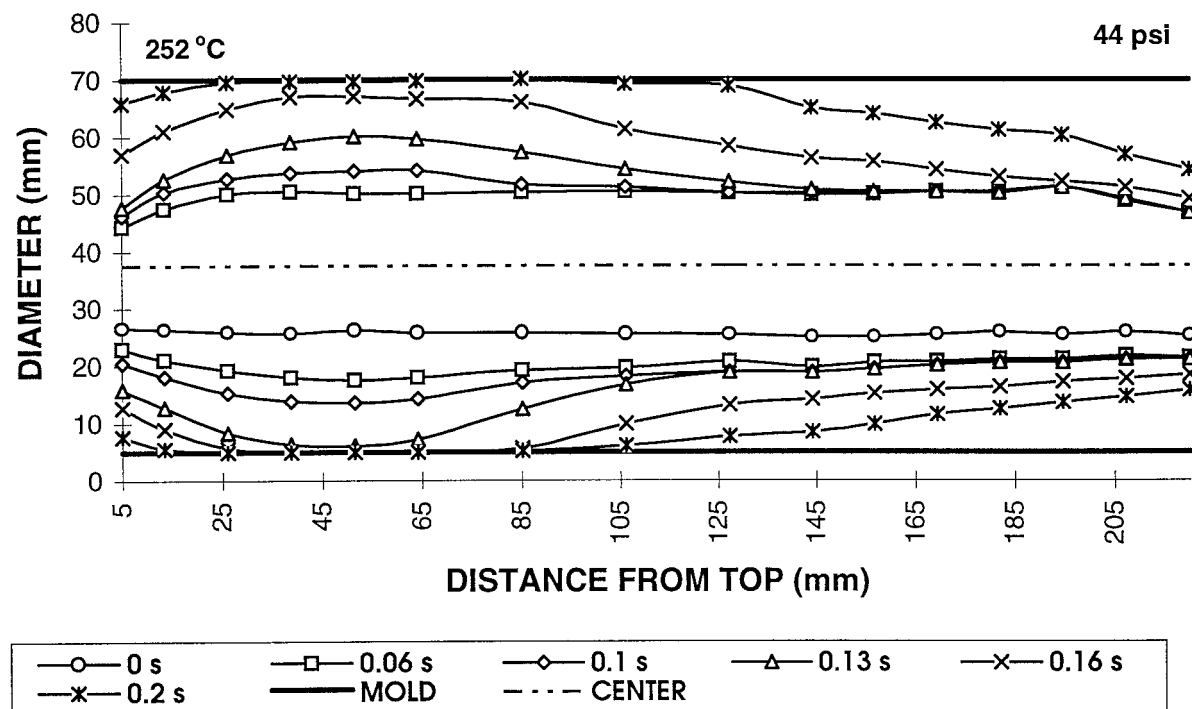


Fig. 13. Parison outside diameter profile during inflation; glass fiber filled polyamide at nominal inflation pressure of 44 psi (0.30 MPa) at 252°C.

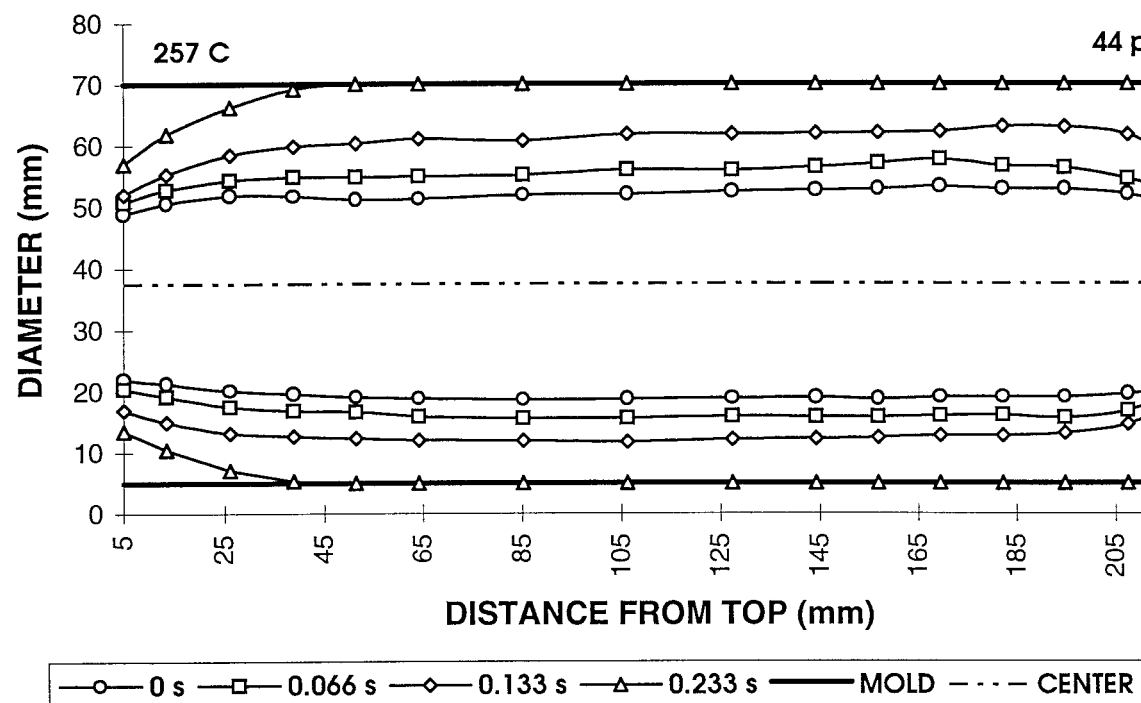


Fig. 14. Parison outside diameter profile during inflation; polyolefin modified polyamide at nominal inflation pressure of 44 psi (0.30 MPa) at 257°C.

Table 2. Durations for the Inflation Process for Different Polyamides.

Resin	Nominal Inflation Pressure (psi)	Time Required to Reach Mold Wall (s)
Neat resin	44 (0.3 MPa)	0.50
Neat resin	100 (0.69 MPa)	0.20
Fiber incorporated	44 (0.3 MPa)	0.20
Fiber incorporated	100 (0.69 MPa)	0.10
Polyolefin modified	44 (0.3 MPa)	0.23
Polyolefin modified	100 (0.69 MPa)	0.14

significant increase in the strain rate during further inflation. Hence, it is possible to have a higher effective strain rate for a lower inflation pressure, as demonstrated by the neat resin. At high inflation pressures, the fiber incorporated resin exhibited the maximum strain rate of 24 s^{-1} observed during the onset of inflation, while the polyolefin modified resin exhibited the lowest strain rate, 4 s^{-1} . The higher Hencky strain rate observed with the fiber incorporated resin should be associated with the relatively low elasticity (i.e., ability to hold shape) of the fiber incorporated resin and also the relatively smaller thicknesses of its parisons. The relatively low value of the strain rate during the inflation of the polyolefin modified resin was similar to the typical strain rate values observed earlier for high-density polyethylene resins, i.e., around 9 s^{-1} (30).

Analysis of the internal pressure data during inflation of the parison reveals a plateau occurring after a few tenths of a second. A similar phenomenon has been observed by Weissmann (44) in stretch blow

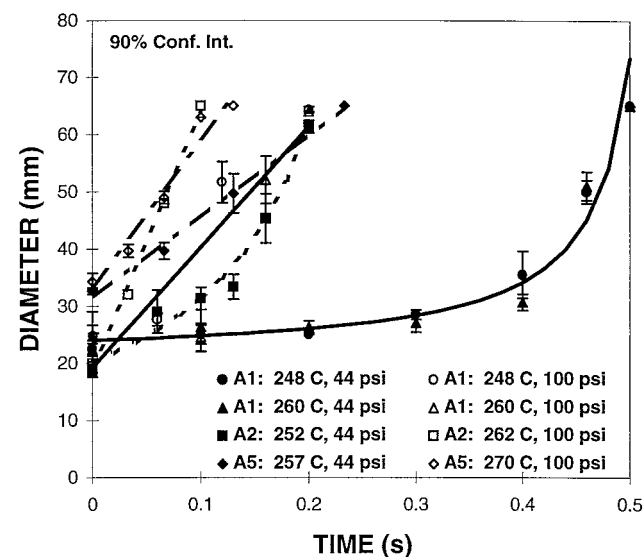


Fig. 15. Parison outside diameter vs. time for three polyamides (A1: neat, A2: glass filled, A5: polyolefin modified) under nominal inflation pressure conditions of 44 psi (0.3 MPa) and 100 psi (0.69 MPa).

molding of PET. The internal parison pressure, pressure against the mold wall (external pressure), and fraction of the parison center that has been inflated are plotted on the same time scale in Fig. 17. "Fraction of parison inflated" refers to the location of the parison in relation to the mold cavity, determined at the center (about 11 cm from the top of the cavity). The fractions 0.3 and 1 refer to the parison locations before inflation and upon the parison contacting the mold cavity, re-

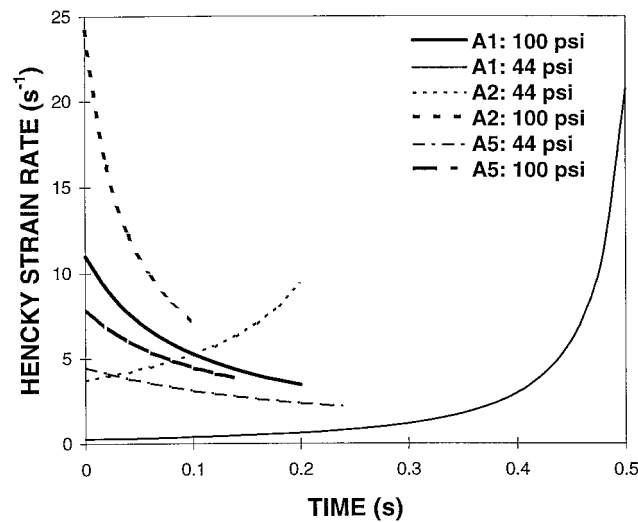


Fig. 16. Hencky strain rate vs. time (A1: neat, A2: glass filled, A5: polyolefin modified) under various nominal inflation pressure conditions of 44 psi (0.3 MPa) and 100 psi (0.69 MPa).

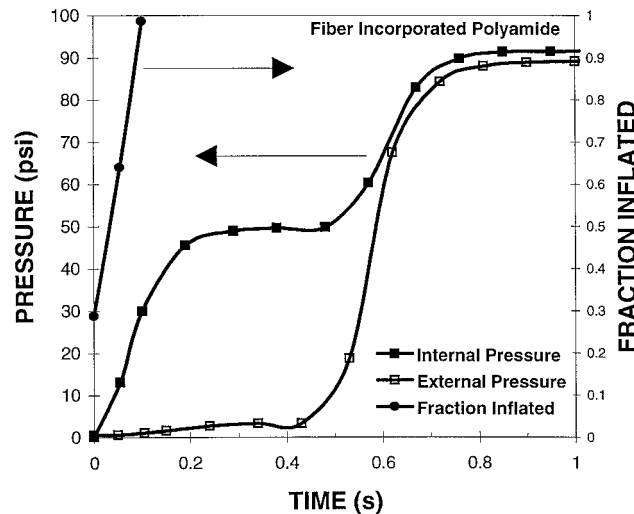


Fig. 17. Pressure inside the parison during inflation, pressure in the cavity outside the parison during inflation (0 to 100 psi or 0 to 0.69 MPa) and fraction of the parison inflated at the center of the cavity for glass fiber filled polyamide.

spectively. The inflation of the rest of the parison continues until all of the cavity is filled. The center of the parison begins to expand radially as soon as air is supplied and internal pressure builds, accompanied by a small increase in the pressure between the parison and the mold due to the compression of the air trapped between the parison and the mold wall. Once the center of the parison has reached the mold wall, it begins to expand very rapidly biaxially (see Figs. 13 and 14). The biaxial propagation and the accompanying volume change occur so rapidly that the internal pressure in the parison levels off. Once the parison fills the mold completely, the external and internal pressures rise to the nominal supply pressure. As previously observed by Haessly and Ryan (25), it is important to note that the pressure at which inflation

occurs is substantially lower than the nominal inflation pressure set by the operator.

Since the internal pressure of the parison is known during inflation, it is possible to calculate the hoop stress experienced by the center of the parison during inflation. Employing the thin shell approximation, the hoop stress of the inflating parison is given by:

$$\sigma(z, t) = \frac{P(t) R(z, t)}{H(z, t)} \quad (6)$$

where $\sigma(z, t)$ is the hoop stress, $P(t)$ is the internal pressure during inflation, $R(z, t)$ is the parison radius, $H(z, t)$ is the parison thickness, z is the axial distance from the die, and t is the time. The thickness of the inflating parison as a function of time can be computed from

$$H(z, t) = \frac{D_2(z, t) - D_1(z, t)}{2} \\ = \frac{D_2(z, t)}{2} - \frac{1}{2} \left[D_2^2(z, t) - \frac{4W_i(z)}{\pi \Delta L \rho} \right]^{1/2} \quad (7)$$

where $D_2(z, t)$ is the outside diameter of the parison, $D_1(z, t)$ is the inside diameter of the parison, $W_i(z)$ is the weight of the i th pillow at axial distance z with length ΔL (from the pinch-off mold), and ρ is the density of the melt. Figure 18 illustrates the hoop stress experienced by the fiber incorporated resin at high and low nominal inflation pressures as well as the hoop stress for a HDPE inflated under similar conditions. The hoop stress for the fiber incorporated resin increases faster than the hoop stress for the HDPE resin but has a lower ultimate value at the completion of inflation.

As illustrated in Fig. 18, where the hoop stress is plotted against strain, the modulus of the inflating parison is not constant but rather a function of total strain, particularly at the highest inflation pressures.

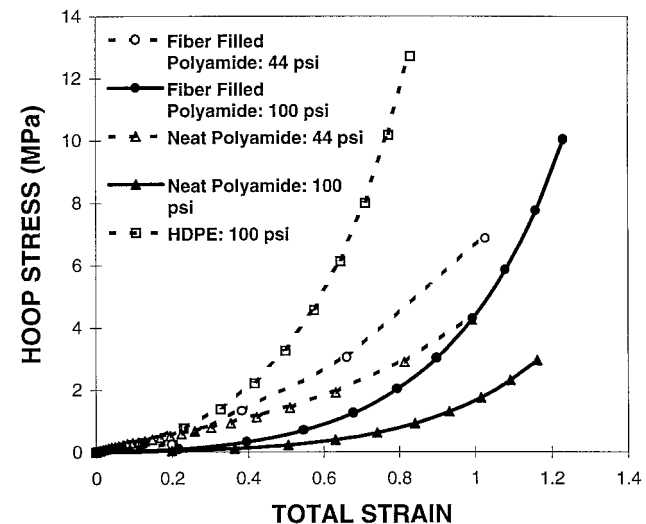


Fig. 18. Hoop stress vs. total strain during radial expansion of the inflating parison at the nominal inflation pressures of 44 psi (0.3 MPa) and 100 psi (0.69 MPa).

It is seen that the modulus of the inflating parison is smaller for the fiber incorporated polyamide in comparison with the parison for high-density polyethylene.

CONCLUSIONS

Three polyamide resins were blow molded using a conventional continuous blow molding machine. Although storage modulus and first normal stress difference values are similar for the neat and fiber filled polyamide 6 resins, the presence of the fibers drastically reduces the ability of the fiber incorporated polyamide to hold its shape. This is manifested in the reduced extrudate swell and increased drawdown during parison formation and consequently the small wall thickness of the parisons and blown parts. Owing to lack of significant swelling of the fiber incorporated resin, it is necessary to employ a larger die gap for parison formation. On the other hand, the polyolefin modified resin resists sagging and necking better than the other two resins, making it more suitable for large parts. Further, the inflation behavior of the polyolefin modified resin was more consistent across a range of inflation pressures, while the neat and fiber incorporated resins inflated differently at different pressures. The pressure at which inflation occurs is related to the supply (nominal) pressure but occurs at a much lower value. The presented parison formation and inflation data for the three resins should provide a better understanding of the blow molding behavior of polyamide resins.

ACKNOWLEDGMENTS

The authors would like to acknowledge the contributions of Messrs. Thomas J. Krolick and Daniel S. Leydon of AlliedSignal Corporation for supplying the resin and processing information and Mobil Chemical Company for permitting the use of their equipment. Dr. Paul Tong and Dr. Pradeep P. Shirodkar of Mobil Chemical Company provided valuable guidance during the course of experiments and manuscript preparation. The funding of AlliedSignal Inc., and Mobil Chemical Company is gratefully acknowledged.

REFERENCES

1. D. Kalyon, V. Tan, and M. Kamal, *Polym. Eng. Sci.*, **20**, 773 (1980).
2. A. Garcia-Rejon and J. M. Dealy, *Polym. Eng. Sci.*, **22**, (1982).
3. N. Orbey and J. Dealy, *Polym. Eng. Sci.*, **24**, 511 (1984).
4. D. M. Kalyon and M. R. Kamal, *Polym. Eng. Sci.*, **26**, 504 (1986).
5. R. J. Koopmans, *Polym. Eng. Sci.*, **32**, 1755 (1992).
6. R. W. DiRaddo and A. Garcia-Rejon, *Can. J. Chem. Eng.*, **71**, 5, 824 (1993).
7. M. Kamal, V. Tan, and D. Kalyon, *Polym. Eng. Sci.*, **21**, 331 (1981).
8. X.-L. Luo and E. J. Mitsoulis, *J. Rheol.*, **33**, 8, 1307 (1989).
9. X.-L. Luo and R. I. Tanner, *J. Non-Newton. Fluid Mech.*, **22**, 61 (1986).
10. X.-L. Luo and R. I. Tanner, *Int. J. Num. Meth. Eng.*, **25**, (1988).
11. Y. C. Ahn and M. E. Ryan, *Int. J. Numer. Meth. Fluids*, **13**, 10, 1289 (1991).
12. P. Brousseau, K. Nguyen, and M. R. Kamal, *SPE ANTEC Tech. Papers*, **37**, 1429 (1991).
13. Y. C. Ahn and M. E. Ryan, *Comp. Fluids*, **21**, 2, 267 (1992).
14. A. Goublomme, B. Draily, and M. J. Crochet, *J. Non-Newton. Fluid Mech.*, **44**, 171 (1992).
15. E. Mitsoulis and H. J. Park, *Theor. Appl. Rheol., Proc. Int. Congr. Rheol.*, 11th, **Vol. 1**, 385 (1992).
16. D. G. Kiriakidis and E. Mitsoulis, *Adv. Polym. Tech.*, **12**, 2, 107 (1993).
17. A. Goublomme and M. J. Crochet, *J. Non-Newton. Fluid Mech.*, **47**, 281 (1993).
18. J. R. Clermont and M. Normandin, *J. Non-Newton. Fluid Mech.*, **50**, 2/3, 193 (1993).
19. R. Y. Chang and W. L. Yang, *J. Non-Newton. Fluid Mech.*, **51**, 1, 1 (1994).
20. G. Barakos and E. Mitsoulis, *J. Non-Newton. Fluid Mech.*, **58**, 2/3, 315 (1995).
21. Y. Sasaki, M. R. Kamal, I. Ansari, W. Frydrychowicz, and M. E. Ryan, *SPE ANTEC Tech. Papers*, **40**, 1212 (1994).
22. R. Ahmed, R. F. Liang, and M. R. Mackley, *J. Non-Newton. Fluid Mech.*, **59**, 2/3, 129 (1995).
23. N. Sheptak and C. Beyer, *SPE J.*, **21**, 190 (1965).
24. S. Dormeier, *SPE ANTEC Tech. Papers*, **32**, 796 (1986).
25. W. P. Haessly and M. E. Ryan, *Polym. Eng. Sci.*, **33**, 1279 (1993).
26. R. W. DiRaddo, W. I. Patterson, and M. R. Kamal, *Adv. Polym. Tech.*, **8**, 3, 265 (1988).
27. R. W. DiRaddo and A. Garcia-Rejon, *Polym. Eng. Sci.*, **32**, 1401 (1992).
28. A. Garcia-Rejon, P. Cielo, P. Swan, and M. R. Kamal, *SPE ANTEC Tech. Papers*, **39**, 1885 (1993).
29. P. L. Swan, J. M. Dealy, A. Garcia-Rejon, and Dourdour, *Polym. Eng. Sci.*, **31**, 705 (1991).
30. M. R. Kamal, D. M. Kalyon, and V. Tan, *Rheology—Volume 3: Applications*, Plenum Press, New York (1980).
31. M. Ryan and A. Dutta, *Proc. 2nd World Congress of Chemical Engineering*, **6**, 277 (1981).
32. R. Rivlin, *Phil. Trans. Royal Soc., London, A*, **242**, 2973 (1949).
33. J. Sun, X.-L. Luo, and R. I. Tanner, *Int. Polym. Proc.*, **9**, 2, 168 (1994).
34. B. Coleman, *Proc. Royal Soc. London, A*, **306**, 449 (1968).
35. S. Chung and J. Stevenson, *Rheol. Acta*, **14**, 832 (1975).
36. M. Ryan and A. Dutta, *Polym. Eng. Sci.*, **22**, 569 (1982).
37. J. S. Yu and D. M. Kalyon, *Plastics and Rubber Processing and Applications*, **15**, 95 (1991).
38. H. DeLorenzi and H. Nied, *Computers and Structures*, **26**, 197 (1987).
39. R. W. DiRaddo, A. Garcia-Rejon, and L. Pecora, *Adv. Polm. Tech.*, **13**, 4, 275 (1994).
40. R. W. DiRaddo and A. Garcia-Rejon, *Polym. Eng. Sci.*, **34**, 1080 (1994).
41. T. J. Krolick, *SPE ANTEC Tech. Papers*, **37**, 1465 (1991).
42. R. Yazici, A. Wagner, D. M. Kalyon, and S. B. Han, *SPE ANTEC Tech. Papers*, **40**, 1172 (1994).
43. E. Henze and W. Wu, *Polym. Eng. Sci.*, **13**, 153 (1973).
44. D. Weissmann, *SPE ANTEC Tech. Papers*, **34**, 808 (1988).

Revision received January 1996